Physical Simulation of Dynamic Resistive Switching in Metal Oxides Using a Schottky Contact Barrier Model

A. Marchewka
Institut für Werkstoffe der Elektrotechnik II
RWTH Aachen University
52074 Aachen, Germany
marchewka@iwe.rwth-aachen.de

R. Waser and S. Menzel
Peter Grünberg Institut
Forschungszentrum Jülich
52425 Jülich, Germany

***Abstract*—We present a numerical drift-diffusion model of electronic-ionic transport combined with a Schottky contact barrier model to study resistive switching phenomena in ReRAM devices. Capturing the transition between Schottky and ohmic contact resistances upon temperature-accelerated ion migration, our model correctly describes the quasi-static *I–V* switching characteristics as well as dynamic set and reset events. It is shown to account for a transition between bipolar resistive switching and complementary switching when reducing the asymmetry between the contact barriers. Further, it is used to characterize the abrupt and gradual behavior of the set and the reset process, respectively.**

Keywords—ReRAM, Schottky contact, ion migration, simulation model

I. Introduction

Redox-based random access memory (ReRAM) based on transition metal oxides is considered a promising candidate to replace existing memory technologies due to superior scalability and performance [1]. Yet, key challenges to be overcome for ReRAM in order to become a viable commercial technology are a profound understanding of the governing physical mechanisms and the development of reliable dynamic simulation models. ReRAM cells consist of simple metal-insulator-metal (MIM) structures whose resistance can be switched between different states by electrical stimulation. The switching process as well as the initial electroforming process in transition-metal-oxide-based devices are widely assumed to rely on temperature- and field-activated oxygen-vacancy migration and related redox reactions [1]. So far, only few physics-based numerical models involving temperature- and field-driven ion migration have been employed to study dynamic events such as set and reset transitions or complementary switching (CS) [2-5]. Though changes in the electronic barrier at the electrode-oxide junction are frequently suggested to be substantial to the switching and the electroforming process [6], the effect of an interface contact potential is not included in these approaches.

We present a numerical drift-diffusion model of coupled electronic-ionic transport that accounts for current conduction across the electrode-oxide boundaries via electron tunneling and thermionic emission. This treatment of the electron current across the interface enables a unified simulation of Schottky and ohmic contacts [7], thus accounting for the transition between both upon ion migration and related barrier modification. In this study, the capability of the model to describe the transition between bipolar and complementary resistive switching as well as the set and reset transition is evaluated.

II. Simulation Model

A. Model equations

We consider a one-dimensional representation of the MIM device consisting of a donor-doped oxide layer (donor concentration N_{VO}) confined by electrodes at $x = 0$ and $x = L$. Neglecting the minority carriers and assuming that the donors are twofold ionizable, the Poisson equation reads

$$\nabla\left(\varepsilon_0\varepsilon_\mathrm{r}\nabla\psi\right) = -e\left(n - N_{\mathrm{VO}}^{+} - 2N_{\mathrm{VO}}^{2+}\right). \quad (1)$$

It is solved self-consistently with the steady-state drift-diffusion equation for electrons

$$\nabla\left(\mu_n n\nabla\psi - D_n\nabla n\right) = \pm\frac{\partial j_{n,\mathrm{tunnel}}}{\partial x} \quad (2)$$

in an inner loop. In (1) and (2), ε_0 is the free-space permittivity, ε_r is the relative permittivity of the oxide, ψ is the potential, n is the electron concentration, N_{VO}^{+} (N_{VO}^{2+}) is the concentration of the singly (doubly) ionized donors, μ_n is the electron mobility and D_n is the electron diffusion coefficient. The term on the right-hand-side of (2) describes a local generation/recombination rate due to electron tunneling through the contact potential barriers with $j_{n,\mathrm{tunnel}}$ being the tunneling current density. The positive sign and negative sign corresponds to carrier creation behind and carrier annihilation in front of the barrier, respectively. With the new potential values, the time-dependent drift-diffusion equation for the doubly ionized dopants

$$\frac{\partial N_{\mathrm{VO}}^{2+}}{\partial t} - \nabla\left(\mu_{\mathrm{VO}}N_{\mathrm{VO}}^{2+}\nabla\psi + D_{\mathrm{VO}}\nabla N_{\mathrm{VO}}^{2+}\right) = -R_{\mathrm{VO},2} \quad (3)$$

978-1-4673-7860-4/15/$31.00 ©2015 IEEE

is solved using an implicit time-stepping scheme. As a boundary condition for (3), the ionic current across the contacts is assumed to vanish. For the same time step, the rate equations

$$\frac{\partial N_{\mathrm{VO}}^{+}}{\partial t} = -R_{\mathrm{VO},1}, \tag{4}$$

$$\frac{\partial N_{\mathrm{VO}}^{0}}{\partial t} = -R_{\mathrm{VO},0} \tag{5}$$

are solved to obtain the concentrations of the singly ionized and neutral dopants. In the above equations, μ_{VO} is the donor mobility, D_{VO} is the donor diffusion coefficient, and $R_{\mathrm{VO},2}$, $R_{\mathrm{VO},1}$ and $R_{\mathrm{VO},0}$ represent the recombination rates that are derived from the laws of mass action for the ionization reactions along with the dopant ionization statistics [8]. The mobility and diffusion coefficient in (2) and (3) are assumed to be related to each other by the Einstein relation. Further, the donor diffusion is assumed to be temperature-activated obeying an Arrhenius law

$$D_{\mathrm{VO}} = D_0 \exp\left(-\frac{\Delta H_{\mathrm{D,VO}}}{k_{\mathrm{B}} T}\right)\left(1-\frac{N_{\mathrm{VO}}^{2+}}{N_{\mathrm{VO,max}}}\right). \tag{6}$$

Here, k_{B} is the Boltzmann constant, D_0 is the diffusion-coefficient prefactor, $\Delta H_{\mathrm{D,VO}}$ is the activation enthalpy for diffusion, and $N_{\mathrm{VO,max}}$ is the maximum possible donor concentration in the oxide layer. The temperature in the structure is taken to be uniform. It is estimated using the filament's thermal resistance with an equivalent thermal conductivity value κ of the filament in one-dimensional approximation, yielding

$$T = 300\ \mathrm{K} + \frac{L}{8\kappa} j_{\mathrm{mean}} V_{\mathrm{device}}, \tag{7}$$

where j_{mean} describes the mean value of the current density in the insulating layer (including electronic and ionic current contributions) and V_{device} is the voltage drop across the layer.

B. Schottky contact barrier model

The electron current across the metal–insulator contacts is modelled in terms of a thermionic emission contribution and a tunneling contribution. The first is calculated as a current boundary condition at $x_i = \{0, L\}$ according to

$$j_{\mathrm{TE}}(x_i) = \frac{A^* T}{k_{\mathrm{B}}} \int_{E_{\mathrm{C}}(x_i)}^{\infty} N_{\mathrm{supply}}(E_x)\, dE_x, \tag{8}$$

while the latter is calculated as

$$j_{\mathrm{tunnel}}(x) = \frac{A^* T}{k_{\mathrm{B}}} \int_{E_{\mathrm{C,min}}(x)}^{E_{\mathrm{C,max}}(x)} \mathcal{T}(E_x)\, N_{\mathrm{supply}}(E_x)\, dE_x \tag{9}$$

and implemented as a local rate in the recombination term of the drift-diffusion equation (2) as outlined in [7, 9]. In (8) and (9), A^* denotes the Richardson constant, $N_{\mathrm{supply}}(E_x)$ the supply function that describes the supply with carriers and is derived by integration of the occupancy function on both sides of the barrier, and $\mathcal{T}(E_x)$ is the transmission coefficient that is calculated using the WKB approximation. The integration is performed over all energies from the conduction band edge E_{C} onwards for the thermionic emission contribution, and over the local energy difference across the control volume of the discretized domain for the tunneling contribution. Image-force induced barrier lowering is accounted for in the boundary conditions for the Poisson equation (1), which are expressed as

$$\psi(x_i) = \psi_{\mathrm{i}}^{0} + \frac{k_{\mathrm{B}} T}{e} \eta_{\mathrm{Fn}}^{0} - \phi_{\mathrm{Bn}}(x_i) + \psi_{\mathrm{a}}(x_i), \tag{10}$$

with ψ_{i}^{0} being the intrinsic potential in the undisturbed semi-conductor and η_{Fn}^{0} the energy difference between the bottom of the conduction band and the Fermi level, normed by $k_{\mathrm{B}}T/e$. The term $\phi_{\mathrm{Bn}}(x_i)$ denotes the effective potential barrier height at the contact and can be described as

$$\phi_{\mathrm{Bn}}(x_i) = \phi_{\mathrm{Bn0}}(x_i) \mp \Delta\phi_{\mathrm{Bn}}(x_i) \approx \phi_{\mathrm{Bn0}}(x_i) \mp \sqrt{\frac{e\left|\frac{d\psi(x_i)}{dx}\right|}{4\pi\varepsilon_0\varepsilon_{\mathrm{opt}}}} \tag{11}$$

with $\phi_{\mathrm{Bn0}}(x_i)$ being the nominal potential barrier height and $\varepsilon_{\mathrm{opt}}$ the high-frequency relative permittivity. In (12), the negative sign corresponds to the case where the potential gradient is negative at the contact interface $x = 0$ (positive at $x = L$), leading to an effective barrier lowering, while the positive sign corresponds to the opposite potential gradient, leading to barrier enhancement.

TABLE I. SIMULATION PARAMETERS

Symbol	Value	Symbol	Value
L	10 nm	D_0	$1\times10^{-4}\ \mathrm{m^2 s^{-1}}$
ε_{r}	20	$\Delta H_{\mathrm{D,VO}}$	1.0 eV
$\varepsilon_{\mathrm{opt}}$	5.5	$N_{\mathrm{VO,max}}$	$5\times10^{22}\ \mathrm{cm^{-3}}$
κ	$1.25\ \mathrm{W(mK)^{-1}}$	μ_n	$5.5\ \mathrm{cm^2 (Vs)^{-1}} (T/(300\ \mathrm{K}))^{-2.23}$

III. SIMULATION RESULTS

A. Quasi-Static I–V Characteristics

Simulations of quasi-static *I–V* sweeps are performed for different combinations of contact barrier heights, cf. Fig. 1. The physical parameters used in the simulations are given in Table 1. The simulations start with a uniform initial donor distribution of $N_{\mathrm{VO}} = 1\times10^{21}\ \mathrm{cm}^{-3}$. Two triangular voltage sweeps of ±1.5 V amplitude are performed, starting with the positive polarity applied to the interface at $x = 0$. Generally, the curves of the first (black line in Fig. 1) and second (blue line) sweep overlap after the first reset, which occurs on the rising pulse edge of the first sweep. The characteristic of the second sweep thus does not depend on the initial donor distribution anymore and will be discussed in the following. Fig. 1(a) shows the resulting *I–V* characteristic for an asymmetric structure with barrier heights $e\phi_{\mathrm{Bn0}}(0) = 0.7\ \mathrm{eV}$ and $e\phi_{\mathrm{Bn0}}(L) = 0.1\ \mathrm{eV}$. The curve exhibits pure bipolar switching with the structure being turned from a low resistive state (LRS) into a high resistive state (HRS) with the positive voltage polarity (reset process) and switched back to the LRS with the

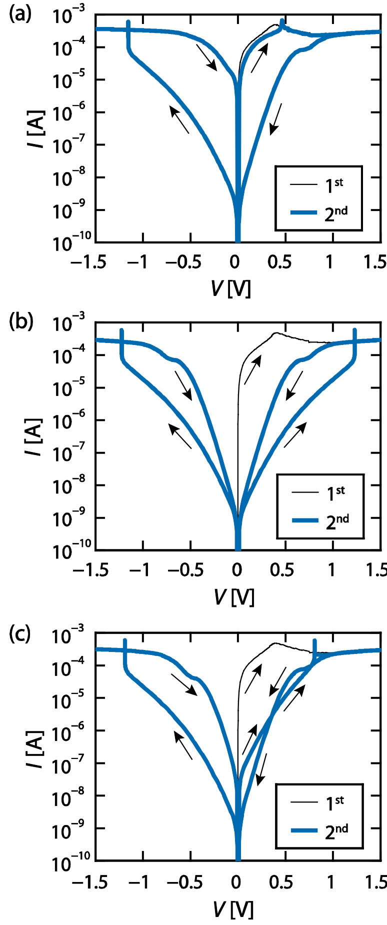

Fig. 1. I–V characteristics of (a) an asymmetric structure exhibiting bipolar resistive switching, (b) a symmetric structure exhibiting the sense of rotation of CS, and (c) a slightly asymmetric structure indicating a transition between bipolar resistive switching and CS.

negative polarity (set process). The I–V characteristic for a symmetrical structure with barrier heights $e\phi_{\mathrm{Bn0}}(0) = e\phi_{\mathrm{Bn0}}(L) = 0.7$ eV in Fig. 1(b) shows symmetrical behavior. The sense of rotation is the same as observed in complementary switching structures. In Fig. 1(c), the I–V characteristic for a slightly asymmetric structure with $e\phi_{\mathrm{Bn0}}(0) = 0.7$ eV and $e\phi_{\mathrm{Bn0}}(L) = 0.5$ eV is depicted. The crossing of the branches in the positive voltage polarity range indicates a transition from bipolar to complementary switching for this electrode configuration. These results support the experimental findings on the dependence of the switching mode on the Ta layer thickness in Ta/TaO_x/Pt structures suggesting the work-function asymmetry between the electrodes to be the switching-mode-controlling parameter [10].

B. Set and Reset Transition

Studies on the capability of the model to describe the set and reset transition of the bipolar switching structure are shown in Fig. 2 and Fig. 3. The set kinetics of the bipolar switching structure with barrier heights $e\phi_{\mathrm{Bn0}}(0) = 0.7$ eV and

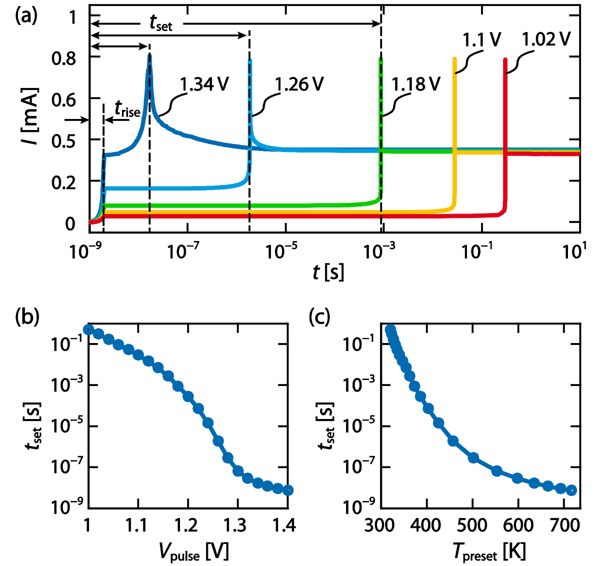

Fig. 2. (a) Transient currents during set operation upon voltage pulse excitation with different amplitudes V_{pulse} for a bipolar switching structure, (b) Set time as a function of applied voltage, (c) Relationship between set time and temperature T_{preset} in the oxide layer before the set operation.

$e\phi_{\mathrm{Bn0}}(L) = 0.1$ eV is investigated by calculating the current response to a voltage step with rise time of 2 ns and varying amplitude. Starting point of this calculation is the donor distribution after a half-sweep with positive voltage polarity. Fig. 2(a) shows set transients for pulse voltages between 1.02 V and 1.34 V, with corresponding set times t_{SET} reaching from several tens of seconds to several nanoseconds. The typical ultra-nonlinear relation between the set time and the set voltage is depicted in Fig. 2(b) and exhibits a mean slope of 40 mV/dec. The origin of the set kinetics' nonlinearity has been shown to be attributed to a local temperature increase leading to enhanced ion mobility [11]. The set times are shown as a function of T_{preset} in Fig. 2(c). Here, T_{preset} represents the temperature before the set operation, evaluated after the 2 ns rising edge of the voltage pulse. Depending on the applied voltage, T_{preset} lies between 320 K and 716 K. In conjunction with (6), this results in the observed set times spanning more than 9 orders of magnitude. The strong correlation between the set times and the local temperature increase due to Joule heating has also been revealed in experimental studies showing that the set times are dictated by dissipated thermal power rather than by applied voltage [12-14].

The gradual reset transition and its dependence on the initial donor distribution are characterized in Fig. 3(a). Here, after a first full sweep of ±1.5 V amplitude, positive triangular half-sweeps with increasing reset stop voltage $V_{\mathrm{stop}} = \{0.6$ V, 0.7 V, 0.8 V, 0.9 V, 1.5 V$\}$ are calculated, resulting in different resistance values. The I–V curve for a half-sweep's rising edge overlaps with the I–V curve from the falling edge of the preceding half-sweep. Finally, the impact of the reset stop voltage V_{stop} on the subsequent set voltage is demonstrated in Fig. 3(b). The applied voltage pattern consists of a first full sweep of ±1.5 V amplitude, followed by sweeps with

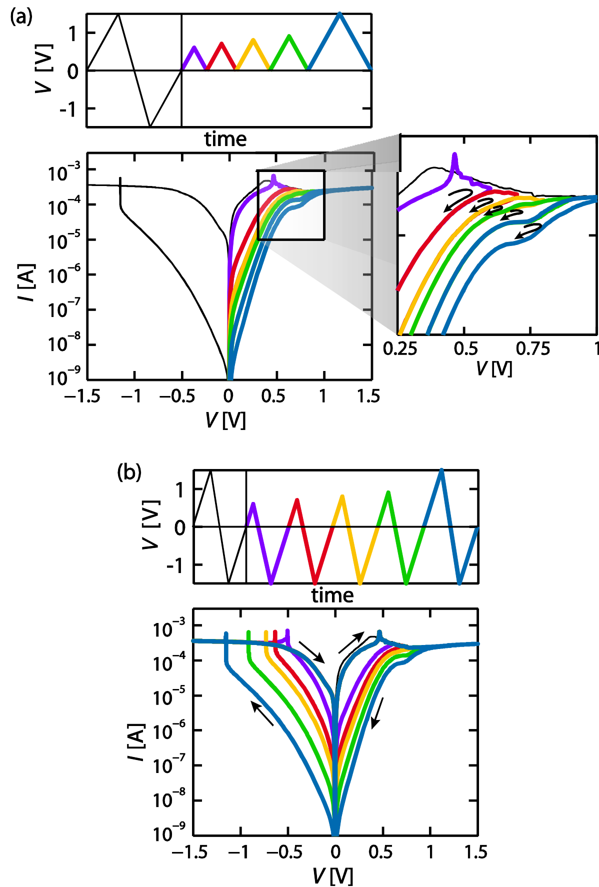

Fig. 3. (a) *I–V* characteristics obtained by applying positive half-sweeps of different amplitudes V_{stop} showing the gradual reset transition, (b) *I–V* characteristics for varying V_{stop} with a subsequent set showing the dependence of the set voltage on the reset stop voltage.

increasing reset stop voltage V_{stop} = {0.6 V, 0.7 V, 0.8 V, 0.9 V, 1.5 V} and constant negative voltage of −1.5 V. The set voltage increases with increasing preceding V_{stop}, since the higher resistance after reset leads to lower temperatures in the following set process, delaying the onset of this transition. The method of controlling the resistance of the HRS by varying V_{stop} has also been demonstrated experimentally [2, 8, 15]. In contrast to the set operation, the driving force of the reset process decreases during the operation. This involves a temperature decrease, leading to deceleration of the ion migration according to (6) and resulting in a gradual reset behavior [2, 8].

IV. Conclusion

In summary, a dynamic numerical model of resistive switching devices is presented that involves electronic barrier modification upon ion migration. It captures the abrupt set and gradual reset characteristics of bipolar resistive switching as well as the transition to complementary switching when reducing the asymmetry between the barriers, offering new insights into the physics of resistive switching.

Acknowledgment

This work was supported in parts by the Deutsche Forschungsgemeinschaft (SFB 917).

References

[1] R. Waser, R. Dittmann, G. Staikov, and K. Szot, "Redox-based resistive switching memories – Nanoionic mechanisms, prospects, and challenges," *Adv. Mater.*, vol. 21, pp. 2632-2663, 2009.

[2] S. Larentis, F. Nardi, S. Balatti, D. C. Gilmer, and D. Ielmini, "Resistive switching by voltage-driven ion migration in bipolar RRAM – Part II: Modeling," *IEEE Trans. Electron Devices*, vol. 59, pp. 2468-2475, 2012.

[3] F. Nardi, S. Balatti, S. Larentis, D. C. Gilmer, and D. Ielmini, "Complementary switching in oxide-based bipolar resistive-switching random memory," *IEEE Trans. Electron Devices*, vol. 60, pp. 70-77, 2013.

[4] S. Kim *et al.*, "Physical electro-thermal model of resistive switching in bi-layered resistance-change memory," *Scientific Reports*, vol. 3, p. 1680, 2013.

[5] S. Kim, S. Choi, and W. Lu, "Comprehensive physical model of dynamic resistive switching in an oxide memristor," *ACS Nano*, vol. 8, pp. 2369-2376, 2014.

[6] J. J. Yang, M. D. Pickett, X. Li, D. A. A. Ohlberg, D. R. Stewart, and R. S. Williams, "Memristive switching mechanism for metal/oxide/metal nanodevices," *Nat. Nanotechnol.*, vol. 3, pp. 429-433, 2008.

[7] K. Matsuzawa, K. Uchida, and A. Nishiyama, "A unified simulation of Schottky and ohmic contacts," *IEEE Trans. Electron Devices*, vol. 47, pp. 103-108, 2000.

[8] A. Marchewka *et al.*, "Nanoionic resistive switching memories: On the physical nature of the dynamic reset process," *unpublished*, 2015.

[9] M. Ieong, P. Solomon, S. Laux, H. Wong, and D. Chidambarrao, "Comparison of raised and Schottky source/drain MOSFETs using a novel tunneling contact model," *IEEE International Electron Devices Meeting (IEDM) Technical Digest*, pp. 733-736, 1998.

[10] A. Schönhals *et al.*, "Critical ReRAM stack parameters controlling complementary versus bipolar resistive switching," *7th IEEE International Memory Workshop (IMW), Monterey*, 2015.

[11] S. Menzel, M. Waters, A. Marchewka, U. Böttger, R. Dittmann, and R. Waser, "Origin of the ultra-nonlinear switching kinetics in oxide-based resistive switches," *Adv. Funct. Mater.*, vol. 21, pp. 4487-4492, 2011.

[12] K. Fleck, U. Böttger, R. Waser, and S. Menzel, "Interrelation of sweep and pulse analysis of the set process in $SrTiO_3$ resistive switching memories," *IEEE Electron Device Lett.*, vol. 35, pp. 924-926, 2014.

[13] Y. Nishi, S. Menzel, K. Fleck, U. Boettger, and R. Waser, "Origin of the set kinetics of the resistive switching in tantalum oxide thin films," *IEEE Electron Device Lett.*, vol. 35, pp. 259-261, 2014.

[14] S. Menzel, M. Salinga, U. Böttger, and M. Wimmer, "Physics of the switching kinetics in resistive memories," *Adv. Funct. Mater.*, 2015, DOI: 10.1002/adfm.201500825.

[15] L. Zhao *et al.*, "Multi-level control of conductive nano-filament evolution in HfO_2 ReRAM by pulse-train operations," *Nanoscale*, vol. 6, pp. 5698-5702, 2014.